

SHAPE AND POSITIONAL GEOMETRY OF MULTI-OBJECT CONFIGURATIONS

JAMES DAMON¹ AND ELLEN GASPAROVIC²

ABSTRACT. In [9], we introduced a method for modeling a configuration of objects in 2D and 3D images using a mathematical “medial/skeletal linking structure.” In this paper, we show how these structures allow us to capture positional properties of a multi-object configuration in addition to the shape properties of the individual objects. In particular, we introduce numerical invariants for positional properties which measure the closeness of neighboring objects, including identifying the parts of the objects which are close, and the “relative significance” of objects compared with the other objects in the configuration. Using these numerical measures, we introduce a hierarchical ordering and relations between the individual objects, and quantitative criteria for identifying subconfigurations. In addition, the invariants provide a “proximity matrix” which yields a unique set of weightings measuring overall proximity of objects in the configuration. Furthermore, we show that these invariants, which are volumetrically defined and involve external regions, may be computed via integral formulas in terms of “skeletal linking integrals” defined on the internal skeletal structures of the objects.

1. INTRODUCTION

In many 2D and 3D images, such as medical images, there appears a configuration of objects, and the analysis of objects in the image benefits from modeling the interplay of the different objects’ shapes and their relative positions. First steps for such an approach for medical images was begun by the MIDAG group at UNC led by Pizer, see e.g. [16], [18], [15], [14], and [2]. These results use a modification of the classical Blum medial axis to model the individual regions together with user chosen, somewhat ad hoc, approaches to relating neighboring objects. Results for the Blum medial axis of an individual region, introduced by Blum-Nagel [1], have concerned its generic structure using a number of different approaches (see, e.g., Mather [19], Yomdin [27], Kimia et al [17], Giblin and Kimia [11], [12]), and its computation (see, e.g., for “grassfire flow” Siddiqi et al. [25], the surveys by Pizer et al. [22] and [24] including Voronoi methods, and for b-splines, Musuvathy et al. [21]). The modification uses methods from “skeletal structure” models for objects as single regions with smooth boundaries (for 2D and 3D see [5] or [7] and more

1991 *Mathematics Subject Classification.* Primary: 53A07, 58A35, Secondary: 68U05.

Key words and phrases. Blum medial axis, skeletal structures, spherical axis, Whitney stratified sets, medial and skeletal linking structures, generic linking properties, model configurations, radial flow, linking flow, measures of closeness, measures of significance, proximity matrix, proximity weights, tiered linking graph.

(1) Partially supported by the Simons Foundation grant 230298, the National Science Foundation grant DMS-1105470 and DARPA grant HR0011-09-1-0055. (2) This paper contains work from this author’s Ph. D. dissertation at Univ. of North Carolina.

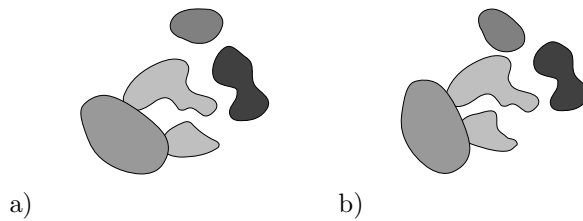


FIGURE 1. Images exhibiting configurations of five objects. A basic problem is to determine the differences between the configurations that are due to changes in the shapes of the objects versus those due to position changes. Furthermore, one would want to find numerical invariants which measure these differences.

generally [3], [4]). These results add considerable flexibility and stability to the classical Blum medial axis.

In [9] we introduced for configurations of objects in \mathbb{R}^2 or \mathbb{R}^3 medial/skeletal linking structures which capture both the shapes of the individual objects and their relative positions in the configuration. In this paper we develop an approach to the “positional geometry” of a configuration using mathematical tools defined in terms of the linking structure, which build upon the methods already developed for skeletal structures for single regions. Moreover, we will see that certain constructions and operators defined for skeletal structures and used for determining the geometry of individual objects can be extended to give simultaneously the positional geometric properties of the entire configuration. As such this provides a natural progression from individual objects to configurations of objects.

Given a collection of configurations, we may ask what are the statistically meaningful shared geometric properties of the collection of configurations, and how the geometric properties of a particular configuration differ from those for the collection. To provide quantitative measures for these properties, we will directly associate geometric invariants to a configuration. Such invariants may be globally defined depending on the entire configuration or locally defined invariants depending on local subconfigurations associated to each object.

For example, if we view the union of the objects as a topological space, then we can measure the Gromov-Hausdorff distance between two such configurations. We may also use the geodesic distance between the two configurations measured in a group of global diffeomorphisms mapping one configuration to another. Such invariants give a single numerical global measure of differences between two configurations. Instead, we will use skeletal linking structures associated to the configurations to directly associate both global and local geometric invariants which can be used to measure the differences between a number of different features of configurations in a variety of different ways.

In introducing these invariants, we will be guided by several key considerations. The first involves distinguishing between the differences in the shapes of individual objects versus their positional differences and how each of these contributes to the differences in the configurations, as illustrated in Figure 1. A first question for objects that do not touch is when they should be considered “neighbors” and what should be the criterion? Second, in measuring the relative positions of neighboring objects, more than just the minimum distance between their boundaries is required;

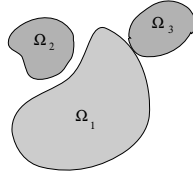


FIGURE 2. Measuring closeness of objects in a configuration. Although Ω_3 touches Ω_1 , only a small portion of Ω_3 is close to Ω_1 . In contrast, Ω_2 does not touch Ω_1 , but it remains close over a larger region. Measuring closeness requires including both of these contributions, both locally and globally.

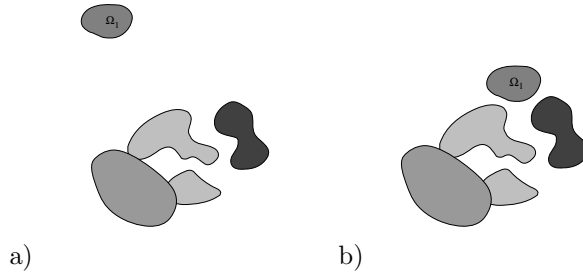


FIGURE 3. Images exhibiting configurations of five objects. In a), Ω_1 is a greater distance from the remaining objects, and hence is less significant when modeling positions within the configuration. In b), the closeness of object Ω_1 to the other objects makes it more significant for modeling the positions within the configuration.

we also wish to measure how much of the regions are close, see, e.g., Figure 2. A goal is then to define numerical measures of *closeness of objects* which takes into account both aspects.

Third, we seek a measure to distinguish how significant are objects within the configuration and to identify those that are mainly outliers. This would provide for a configuration a *hierarchical structure for the objects*, indicating which objects are most central to the configuration and which are less *positionally significant*. For example, in Figure 3, the position of object Ω_1 makes it more important for the overall configuration in b) than in a), where it is more of an “outlier.” A small movement of Ω_1 in a) would be less noticeable and have a smaller effect to the overall configuration than in b). By having a smaller effect we mean that the deformed configuration could be mapped to the original by a diffeomorphism which has smaller local distortions near the configuration in the case of a) versus b). Finally, there is the question of whether there are numerical invariants which can be used to determine when there are identifiable subconfigurations. An example of this is seen in Figure 4.

In Sections 2 and 3 we consider the “linking flow” associated to the linking structure. The nonsingularity of the linking flow is guaranteed in §2 by “linking curvature conditions” on the linking functions, given in a form which extends that given in [3, Thm 2.5] for the radial flow. Next, in §3, we use this linking flow to identify both

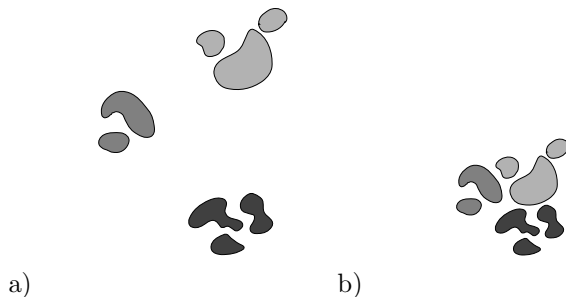


FIGURE 4. Subconfigurations of objects. In a), a configuration is formed from three groups of objects. In b), the groups of objects have been moved closer; based on geometric position, the groups are no longer clearly distinguished.

the internal regions of neighboring objects and external regions shared by them, which are the “linking neighborhoods” between objects. Then, in §4, we show how to compute integrals over the boundaries of the objects or over general regions inside or outside the objects as “medial and skeletal linking integrals,” which are integrals defined on the skeletal sets in the interiors of the objects. Lastly, in §5, we introduce and compute several “volumetric-based” numerical invariants that include measures of the relative closeness of neighboring objects and relative significance of the individual objects. We furthermore show how they may be computed from the medial/skeletal linking structure via skeletal linking integrals.

Then, in §6 we will combine the invariants which measure these geometric features in two different ways. One is to construct a “proximity matrix” which captures the closeness of all objects in the configuration and to which the Perron-Frobenius theorem can be applied, yielding a unique set of “proximity weights” assigned to the objects, measuring their overall closeness in the configuration. The second is to construct a “tiered graph structure,” which is a graph with vertices representing the objects, edges between vertices of neighboring objects, and values of significance assigned to the vertices, and closeness assigned to the edges. Then, as thresholds for closeness and significance vary, the resulting subgraph satisfying the conditions will exhibit the central objects (and outliers) of the configuration, various subgroupings of objects and a hierarchical ordering of the relations between objects. The skeletal linking structure also allows for the comparison and statistical analysis of collections of objects in \mathbb{R}^2 and \mathbb{R}^3 , extending the analyses given in earlier work for single objects.

2. LINKING FLOW AND CURVATURE CONDITIONS

We model a configuration of objects in 2D or 3D images by a collection of regions $\Omega = \{\Omega_i\}$ in either \mathbb{R}^2 or \mathbb{R}^3 , with each Ω_i modeling one of the objects, whose boundaries \mathcal{B}_i may share common boundary regions (see e.g. [9, Fig. 1 and 2]) and along their edges there are singularities of generic type corresponding to whether the objects are flexible or rigid (see e.g. [9, Fig. 5 and 6]).

Medial/Skeletal Linking Structures. We recall from [9] the definition of a skeletal linking structure $\{(M_i, U_i, \ell_i)\}$ for the multi-object configuration $\{\Omega_i\}$.

First of all, it consists of skeletal structures $\{(M_i, U_i)\}$ for each Ω_i , where each M_i is a stratified set in Ω_i and U_i is a multi-valued vector field on M_i whose vectors end at boundary points in \mathcal{B}_i (see [5] for 2D or 3D regions, or more generally [4]). By M_i being a stratified set we mean for regions in \mathbb{R}^2 it is a disjoint collection of smooth curve segments ending at branching or end points, and for \mathbb{R}^3 , it is a disjoint collection of smooth surface regions, curve segments and points, with the surfaces ending at the curves and points. We may define a stratified set \tilde{M}_i from M_i by replacing points $x \in M_i$ by pairs $(x, U_i(x))$, where $U_i(x)$ varies over the multiple values of U_i at x , with strata formed from strata S_j of M_i together with a choice of smoothly varying values $U_i(x)$ for $x \in S_j$. The mapping $\pi : \tilde{M}_i \rightarrow M_i$ sending $(x, U_i(x)) \mapsto x$ sends the strata \tilde{M}_i to strata of M_i . This has the benefit of being able to consider multi-valued objects on M_i as single-valued objects on \tilde{M}_i .

We express $U_i = r_i \mathbf{u}_i$, where \mathbf{u}_i are multi-valued unit vector fields on M_i . In addition, the ℓ_i are multi-valued “linking functions” defined on M_i , and there are then defined the multi-valued “linking vector fields” $L_i = \ell_i \mathbf{u}_i$ on each M_i . These become single valued on \tilde{M}_i .

There are additional conditions of [9, Def. 3.2] to be satisfied for $\{(M_i, U_i, \ell_i)\}$ to be the skeletal linking structure for $\Omega = \{\Omega_i\}$. Conditions S1 - S3 concern a refinement of the stratification of \tilde{M}_i and the differentiability properties of ℓ_i on the strata of the refinement. Also, the conditions L1 - L4 concern the relations between the linking vector fields from different objects and the nonsingularity of the “linking flows” generated by the linking vector fields. Regions defined by the linking flows are what we use to identify properties of the positional geometry of the configuration.

Nonsingularity of the Linking Flow. The nonsingularity of the radial flow, which occurs within the regions, was established in [3, §4] (and see [5, §2]) using the radial and edge shape operators S_{rad} and S_E , which are multi-valued operators defined on M_i , with S_{rad} defined at all points except the edge points ∂M_i of M_i and S_E defined at these points. These capture the geometric properties of the radial vector field U_i and play an important role in determining the local geometric properties of the boundary and the relative and global geometric properties of the region Ω_i (see [4] and [5, §3, 4]). Although their properties differ from those of the differential geometric shape operators appearing in differential geometry, their eigenvalues κ_{r_i} , the *principal radial curvatures* and generalized eigenvalues κ_{E_i} , the *principal edge curvatures*, play an equally important role.

We next explain how they appear in the sufficient conditions we give for nonsingularity of the linking flow. As well we give formulas for the evolution of the radial and edge shape operators under the linking flow.

Recall [9, (3.1)], the *linking flow* from M_i is defined by

$$(2.1) \quad \lambda_i(x, t) = x + \chi_i(x, t) \mathbf{u}_i(x),$$

where $\mathbf{u}_i(x)$ ranges over all possible values and

$$(2.2) \quad \chi_i(x, t) = \begin{cases} 2tr_i(x) & 0 \leq t \leq \frac{1}{2} \\ 2(1-t)r_i(x) + (2t-1)\ell_i(x) & \frac{1}{2} \leq t \leq 1 \end{cases}.$$

For $0 \leq t \leq \frac{1}{2}$, this flow is the radial flow at twice the speed and it extends the radial flow to the exterior of the regions for $\frac{1}{2} \leq t \leq 1$ and ends at the “linking axis” M_0 . We let $\lambda_{it}(x) = \lambda_i(x, t)$ for each t and refer to λ_{i1} as the *linking mapping* from strata of the refinement of \tilde{M}_i to strata of the linking axis. We refer to the combined union of the λ_{it} for all i by λ_t .

To establish the conditions for the nonsingularity of the linking flow for the skeletal linking structure $\{(M_i, U_i, \ell_i)\}$, we introduce the following two conditions:

- (1) (*Linking Curvature Condition*) For all points $x_0 \in M_i \setminus \partial M_i$ and all values $U_i(x_0)$,

$$\ell_i < \min\left\{\frac{1}{\kappa_{rj}}\right\}$$

for all positive principal radial curvatures κ_{rj} ;

- (2) (*Linking Edge Condition*) For all points $x_0 \in \overline{\partial M}$ (the closure of ∂M),

$$\ell_i < \min\left\{\frac{1}{\kappa_{Ej}}\right\}$$

for all positive principal edge curvatures κ_{Ej} .

In these conditions, the values of ℓ_i and either κ_{rj} or κ_{Ej} are at the same point x_0 and for the same value of $U_i(x_0)$.

The nonsingularity of the linking flow (and the radial flow) for a skeletal linking structure is given by the following.

Theorem 2.1 (Nonsingularity of the Linking Flow). *Let $\{(M_i, U_i, \ell_i)\}$ be a skeletal linking structure in \mathbb{R}^2 or \mathbb{R}^3 which satisfies: the Linking Curvature Conditions and Linking Edge Conditions on all of the strata of all M_i . Then, the radial flow also satisfies the radial curvature and edge curvature conditions on each stratum. Hence, the following properties hold.*

- i) *On each stratum S_j of the refinement of \tilde{M}_i , the linking flow is nonsingular and remains transverse to the radial lines.*
- ii) *Hence, the image W_j of the linking map on S_j is locally a smooth stratum of the same dimension and which may only have nonlocal intersections from distant points in S_j . If there are no nonlocal intersections then W_j is a smooth stratum.*
- iii) *The image of a stratum S_j of \tilde{M}_i under the radial map is a smooth stratum of \mathcal{B}_i of the same dimension.*
- iv) *For both flows, at points of the top dimensional strata, the backward projection along the lines of L_i will locally map strata of \mathcal{B}_i , resp. M_0 , diffeomorphically onto the smooth part of M_i .*
- v) *Thus, if there are no nonlocal intersections, each \mathcal{B}_i will be a piecewise smooth embedded surface.*

The proof of this theorem follows from Proposition 8.1 in [8] and its corollaries along with Theorem 2.5 of [5]; see also [10, Chap. 6].

Evolution of the Shape Operators Under the Linking Flow. We may translate the vectors U_i along the lines of each L_i to the level sets of the linking flow. We may use these translated vectors as a radial vector field on the level set. Hence, for each $1 \leq t \leq 1$ we may define corresponding radial shape operators $S_{rad t}$ on the level sets (curves or surfaces) $\mathcal{B}_t = \lambda_t(M_i)$ in a neighborhood of $\lambda_t(x_0)$. We can

best relate them to the radial or edge shape operators on M_i in terms of their matrix representations. For $x_0 \in M_i \setminus \overline{\partial M}$ and each choice of $U_i(x_0)$, there is a smooth stratum $M_{i,j}$ of M_i containing x_0 in its closure and which smoothly extends through x_0 and a smoothly varying value of U_i defined in a neighborhood of x_0 extending $U_i(x_0)$. We denote the tangent space to this stratum at x_0 by $T_{x_0}M_{i,j}$. For S_{rad} we choose a basis \mathbf{v} for $T_x M_{i,j}$, which is either a single vector $\mathbf{v} = \{v_1\}$ for configurations in \mathbb{R}^2 , or $\mathbf{v} = \{v_1, v_2\}$ for \mathbb{R}^3 . We then let \mathbf{v}' denote the image of \mathbf{v} under $d\lambda_{i,t}$ which is a basis for the tangent space to the level set \mathcal{B}_t at $d\lambda_{i,t}$. At points $x_0 \in \overline{\partial M_i}$ for \mathbb{R}^3 , instead a nonzero vector $v_1 \in T_{x_0}\partial M_{i,j}$ is completed to a basis using $U_i(x_0)$ for the source and the unit normal vector $\mathbf{n}(x_0)$ to $M_{i,j}$ for the target. We denote the resulting matrix representation of S_E by $S_{E,\mathbf{v}}$; but for $t > 0$, it evolves to also become radial shape operators $S_{rad,t}$; and we use a basis \mathbf{v}'' , which is the image of the basis \mathbf{v} of $T_{x_0}\partial M_{i,j}$ under $d\lambda_t(x_0)$ with $\mathbf{n}(x_0)$ adjoined.

Remark 2.2. In the 3D case $S_{\mathbf{v}}$ and $S_{E,\mathbf{v}}$ are 2×2 matrices; while in the 2D case, $S_{\mathbf{v}}$ is a 1×1 matrix formed from the single radial curvature κ_r (see e.g. Examples 2.3 and 2.4 in [5]).

Then, the evolved radial shape operators under the linking flow are given by the following.

Proposition 2.3 (Evolution of the Shape Operators).

Suppose $x_0 \in M_i$ with value $U_i(x_0)$ (with a smooth value of U_i in a neighborhood of x_0). Provided the following conditions are satisfied, the linking flow is nonsingular and the evolved radial shape operator on the level surface $\mathcal{B}_t = \lambda_t(M_i)$ in a neighborhood of $\lambda_t(x_0)$ is given by the following.

- 1) For $x_0 \in M_i \setminus \overline{\partial M}$, if $\frac{1}{\chi(t)}$ is not an eigenvalue of $S_{\mathbf{v}}$ for $0 \leq t \leq 1$, then

$$S_{\mathbf{v}',t} = (I - \chi(t)S_{\mathbf{v}})^{-1}S_{\mathbf{v}}.$$

- 2) For $x_0 \in \overline{\partial M}$, if $\frac{1}{\chi(t)}$ is not a generalized eigenvalue of $(S_{E,\mathbf{v}}, I_{n-1,1})$ for $0 < t \leq 1$, then

$$S_{\mathbf{v}'',t} = (I_{n-1,1} - \chi(t)S_{E,\mathbf{v}})^{-1}S_{E,\mathbf{v}}.$$

The derivation of these results can be found in [8, §7] and [10, Chap. 6] extending the results in [4], or see [5, §2].

Shape Operators on the Boundary and Linking Medial Axis. As a consequence of the corollaries, we can deduce the shape operator for the linking axis M_0 , and in a region where the *partial Blum condition* is satisfied, the differential geometric shape operator on the boundary. First, for the boundary, it is reached at $t = \frac{1}{2}$. If for $x_0 \in M_i$ the radial vector field is orthogonal to \mathcal{B}_i at the point $x' = \lambda(x_0, \frac{1}{2})$, then we say that the skeletal structure (M_i, U_i) satisfies the *partial Blum condition* at x' . If it satisfies the partial Blum condition in a neighborhood of a smooth point of \mathcal{B}_i , then $S_{\mathbf{v}', \frac{1}{2}}$ in Proposition 2.3 gives the differential geometric shape operator for \mathcal{B}_i at x' , and hence completely describes the local geometry of the boundary at x' . This result and its consequences follow from [4, §3] and also see [5, §3].

If instead we consider the image $x' \in M_0$ of $x_0 \in M_i$ under the linking flow, then to such a point there is the corresponding point $x'' = \lambda(x_0, \frac{1}{2}) \in \mathcal{B}_i$. We then have a value of a radial vector field $U_0 = -(\ell_i - r_i)\mathbf{u}_i$ at x' , with ℓ_i , r_i , and \mathbf{u}_i

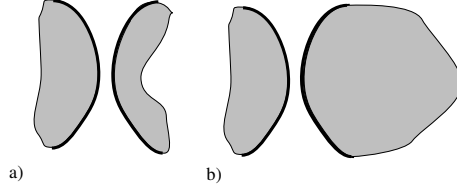


FIGURE 5. Pairs of regions in a) and b) both show the same boundary regions to each other as indicated by the dark curves. However, in b) the region on the right has substantially more volume than does the region on the right in a). This is not captured by neighboring boundary information; however, it is captured using volumetric measures defined from the linking structure.

associated to the value $L_i(x_0)$. This vector at the point x' ends at x'' . This defines a multi-valued vector field U_0 on M_0 . Thus, we can view (M_0, U_0) as a skeletal structure for the exterior region. We can determine the corresponding radial or edge shape operator at x' by the following (see [8, Cor. 8.7]).

Corollary 2.4. *If $x' \in M_0$ is as in the above discussion, then the radial shape operator for the skeletal structure (M_0, U_0) at x' is given by either: if x_0 is a non-edge closure point, then with the notation of Proposition 2.3,*

$$S_{\mathbf{v}'',t} = -(I - \ell_i S_{\mathbf{v}})^{-1} S_{\mathbf{v}};$$

or if x_0 is an edge closure point, then

$$S_{\mathbf{v}'',t} = -(I_{n-1,1} - \ell_i S_{E,\mathbf{v}})^{-1} S_{E,\mathbf{v}}.$$

This follows because the associated unit vector field at x' is $\mathbf{u}_0 = -\mathbf{u}_i$. Thus, the radial shape operator for (M_0, U_0) at x' is the negative of that for the stratum of M_0 , viewed as a level set of the linking flow from $x_0 \in M_0$. Hence, by Proposition 2.3 we obtain the result.

3. POSITIONAL PROPERTIES OF REGIONS DEFINED USING THE LINKING FLOW

We next consider how the medial/skeletal linking structure $\{(M_i, U_i, \ell_i)\}$ for a multi-object configuration $\Omega = \{\Omega_i\}$ in \mathbb{R}^2 or \mathbb{R}^3 allows us to introduce numerical measures capturing various aspects of the object's positions within the configuration. There are two possibilities for this. One is to base the numerical quantities on geometric properties of the boundaries of the objects. The second is to use instead volumetric measures for subregions of the objects and identified regions in the external complement which capture positional information about the objects.

The problem with the first choice is that two regions may show the same boundary region to each other even though there are other pairs of regions showing the same boundaries to each other but which may have completely different shapes and volumes, as shown in Figure 5. The alternative is to keep track of the relation between all points of all boundaries of each pair of regions. However, this involves an enormous redundancy in the data structure. The skeletal linking structure avoids this redundancy, allowing additional geometric information to be computed directly from the linking structure. We also shall see in §4 that for general skeletal linking structures, using volumetric measures to capture positional information will allow

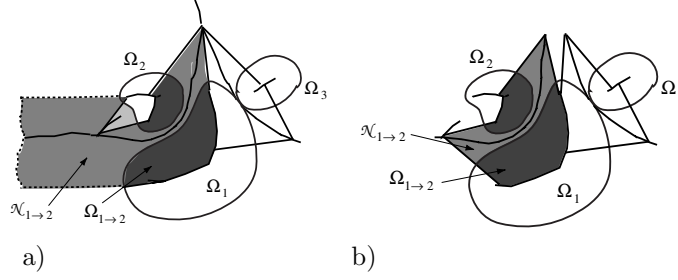


FIGURE 6. Configuration of three regions with portions of the regions Ω_1 and Ω_2 which are linked to each other (darkly shaded regions are parts of $\Omega_{1 \rightarrow 2}$ and $\Omega_{2 \rightarrow 1}$), and their linking neighborhoods (grey shaded regions are parts of $\mathcal{N}_{1 \rightarrow 2}$ and $\mathcal{N}_{2 \rightarrow 1}$). Then, $\mathcal{B}_{1 \rightarrow 2}$ is the portion of the boundary \mathcal{B}_1 where $\mathcal{N}_{1 \rightarrow 2}$ meets $\Omega_{1 \rightarrow 2}$, while $\mathcal{R}_{1 \rightarrow 2}$ is the union of the two regions $\mathcal{N}_{1 \rightarrow 2}$ and $\Omega_{1 \rightarrow 2}$. Note that in the unbounded case in a), much of the linking in the infinite region occurs between small parts of Ω_1 and Ω_2 , and this would not occur for a bounded linking structure in a bounded region as in b) where a threshold is imposed.

us to express these numerical quantities as integrals over the internal skeletal sets M_i of appropriate mathematical quantities derived from the linking structure .

Because finite volumetric measures will require bounded regions in the complement, we will first consider regions defined in the unbounded case and then introduce bounded versions.

Medial/Skeletal Linking Structures in the Unbounded Case. We begin by considering regions Ω_i and Ω_j modeling objects in the configuration that are linked via the linking structure and identifying regions using the linking flow λ_i on each Ω_i . We recall in [9] that Ω_i and Ω_j are said to be “linked” if there are strata $S_{i k}$ in M_i and $S_{j k'}$ in M_j which map to the same stratum in M_0 under the linking flow. We then introduce the following regions as illustrated in Figure 6.

Regions Defined by the Linking Flow:

- i) $M_{i \rightarrow j}$ will denote the union of the strata of \tilde{M}_i which are linked to strata of M_j , and we refer to it as the *strata where M_i is linked to M_j* (the strata being in \tilde{M}_i indicate on which “side” of M_i the linking occurs).
- ii) $\Omega_{i \rightarrow j} = \lambda_i(M_{i \rightarrow j} \times [0, \frac{1}{2}])$ denotes the *region of Ω_i linked to Ω_j* .
- iii) $\mathcal{N}_{i \rightarrow j} = \lambda_i(M_{i \rightarrow j} \times [\frac{1}{2}, 1])$ denotes the *linking neighborhood* of Ω_i linked to Ω_j .
- iv) $\mathcal{B}_{i \rightarrow j} = \Omega_{i \rightarrow j} \cap \mathcal{N}_{i \rightarrow j}$ is the *boundary region of \mathcal{B}_i linked to \mathcal{B}_j* .
- v) $\mathcal{R}_{i \rightarrow j} = \Omega_{i \rightarrow j} \cup \mathcal{N}_{i \rightarrow j}$, is the *total region for Ω_i linked to Ω_j* .

Then, we make a few simple observations. First, $\mathcal{N}_{i \rightarrow j} \cap \mathcal{N}_{j \rightarrow i}$ will consist of the strata of the linking axis M_0 where the linking between Ω_i and Ω_j occurs; and second, the regions for a fixed i but different j may intersect on the images under the linking flow of strata where there is linking between Ω_i and two or more other objects.

Next, strata of M_i may involve “self-linking,” which means different strata of \tilde{M}_i may be linked to each other (see e.g. [9, Fig. 9]). We will still use the notation $M_{i \rightarrow i}$, $\Omega_{i \rightarrow i}$, etc. for the strata, regions etc. involving self-linking. Then, $\mathcal{N}_{i \rightarrow i}$ will intersect $\mathcal{N}_{i \rightarrow j}$ on strata where “partial linking” occurs.

Finally the remaining strata in \tilde{M}_i lie in $M_{i,\infty}$, which is introduced in [9] and consists of the union of strata which are unlinked. By property L_4 in [9, Def. 3.2], the radial flow from the union of the $M_{i,\infty} \times (0, \infty)$ defines a diffeomorphic parametrization of the complement of the regions reached by the linking flow. We may flow at twice the radial flow speed to agree with the linking flow on the rest of \tilde{M}_i . We still refer to this completed flow as the linking flow, and then denote the corresponding regions for $M_{i,\infty}$ by: $\Omega_{i,\infty}$, $\mathcal{N}_{i,\infty}$, $\mathcal{B}_{i,\infty}$ and $\mathcal{R}_{i,\infty}$.

Then, we have the decompositions

$$(3.1) \quad \Omega_i = (\cup_{j \neq i} \Omega_{i \rightarrow j}) \cup \Omega_{i \rightarrow i} \cup \Omega_{i,\infty}$$

with

$$(\cup_{j \neq i} \Omega_{i \rightarrow j} \cup \Omega_{i \rightarrow i}) \cap \Omega_{i,\infty} = \emptyset,$$

but the various $\Omega_{i \rightarrow j}$ and/or $\Omega_{i \rightarrow i}$ may have non-empty intersections, as explained above. There are analogous decompositions for \tilde{M}_i and \mathcal{B}_i . Also, we denote the *total linking neighborhood* by $\mathcal{N}_i = \cup_{j \neq i} \mathcal{N}_{i \rightarrow j}$. Then, $\mathcal{N}_i \cup \mathcal{N}_{i \rightarrow i} \cup \mathcal{N}_{i,\infty}$ is the *total neighborhood of Ω_i* (in the complement of the configuration), whose interior consists of points external to the configuration which are closest to Ω_i .

We let $\mathcal{B}_{i,0}$ denote the portion of the boundary \mathcal{B}_i that is not shared with any other region. We recall that on the strata of \tilde{M}_i corresponding to those in $\mathcal{B}_i \setminus \mathcal{B}_{i,0}$, the linking flow is constant in t for $\frac{1}{2} \leq t \leq 1$. Hence, \mathcal{N}_i at these points only consists of boundary points of $\mathcal{B}_i \setminus \mathcal{B}_{i,0}$. Off of these points we can describe the structure of \mathcal{N}_i using the linking flow. We summarize the consequences of the properties of the linking flow (see [8, Cor. 9.2]).

Corollary 3.1. *For a multi-object configuration $\Omega = \{\Omega_i\}$ with skeletal linking structure $\{(M_i, U_i, \ell_i)\}$, there are the following parametrizations for each region associated to Ω_i by the portions of the level sets of the linking flow in those regions:*

- 1) $\Omega_i \setminus M_i$ is parametrized by the level sets of the linking flow for $0 < t \leq \frac{1}{2}$;
- 2) $\mathcal{N}_i \setminus (\mathcal{B}_i \setminus \mathcal{B}_{i,0})$ is parametrized by the level sets of the linking flow for $\frac{1}{2} \leq t \leq 1$;
- 3) $\mathcal{N}_{i \rightarrow i}$ is parametrized by the level sets of the linking flow for $\frac{1}{2} \leq t < 1$; and
- 4) $\mathcal{N}_{i,\infty}$ is parametrized by the level sets of the radial flow for $1 \leq t < \infty$.

Medial/Skeletal Linking Structures for the Bounded Case. As we have mentioned, because the regions are often unbounded, there is no meaningful numerical measure of their sizes. We can overcome this problem for practical considerations by introducing a bounded region $\tilde{\Omega}$ containing the configuration and such that its boundary $\partial\tilde{\Omega}$ is transverse both to the stratification of M_0 and to the linking vectors on M . In [9], we describe a number of different possibilities for obtaining bounded regions including: a bounding box or bounding convex region, the convex hull of the configuration, a natural or intrinsic bounding region, or a region defined by a user-specified threshold for linking, see, e.g., Figure 8.

Then, we can either truncate the linking vector field, or define it on all of M_i for all $i > 0$ by defining it on M_∞ and subsequently refining the stratification so that the linking vector field ends at $\partial\tilde{\Omega}$ on appropriate strata. This maintains the

nonsingularity of the linking flow as we are merely either reducing ℓ_i or defining L_i on $M_{i,\infty}$.

Thus, we have the corresponding properties from Corollary 3.1, except that for properties 2), 3), and 4) the linking flow and corresponding regions $\mathcal{N}_{i \rightarrow j}$, $\mathcal{N}_{i,\infty}$, and $\mathcal{R}_{i \rightarrow j}$ may only extend to $\partial\tilde{\Omega}$. These regions, which are now compact, are obtained from the unbounded regions by intersecting them with $\tilde{\Omega}$. We refer to this as the bounded case, referring the reader [9, §3] for more details. Moreover, we still obtain analogous formulas for the evolution of the radial shape operators for those level sets of the linking flow while they remain within $\tilde{\Omega}$.

Relevance of the Linking Regions for Positional Geometry. The regions capture various aspects of the positional geometric properties of the configuration. Two regions Ω_i and Ω_j are neighbors if the regions $\Omega_{i \rightarrow j}$, $\mathcal{B}_{i \rightarrow j}$, $\mathcal{N}_{i \rightarrow j}$, etc are nonempty, as are the corresponding $\Omega_{j \rightarrow i}$, etc. Then, the $\mathcal{B}_{i \rightarrow j}$ and $\mathcal{B}_{j \rightarrow i}$ represent the boundary regions “between” these neighbors. Moreover, the $\Omega_{i \rightarrow j}$ and $\Omega_{j \rightarrow i}$ represent the internal portions of the regions which are “closest” to the neighbors. These can be compared to the linking neighborhoods $\mathcal{N}_{i \rightarrow j}$ and $\mathcal{N}_{j \rightarrow i}$ to see how close the neighbors are. The larger the linking neighborhoods are compared to the internal neighboring regions the further away are the neighboring regions. If one region has large linking neighborhoods relative to all of its neighbors, then it plays a less significant positional role for the configuration. This perspective will lead us in §5 to introduce volumetric invariants of these regions which capture this positional geometry. Before doing so, we next explain how numerical volumetric invariants can be obtained from the linking structures using “linking integrals” on the skeletal sets of the regions.

4. GLOBAL GEOMETRY VIA MEDIAL AND SKELETAL LINKING INTEGRALS

We now will use the associated regions we have introduced for a configuration via a skeletal linking structure to define quantitative invariants measuring positional geometry for the configuration. We will do so in terms of integrals which are defined on the internal skeletal sets. We begin by defining these integrals, and then we give a number of formulas for integrals of functions on the regions or boundaries of the configuration in terms of these integrals on the internal skeletal sets (see [8, §10] and for 2D and 3D single regions [7, §3.4]).

In practice, skeletal structures have been modeled discretely, as can be skeletal linking structures. For these the integrals then can be discretely approximated from the linking structure to compute the appropriate numerical invariants.

Defining Medial and Skeletal Linking Integrals. We begin by considering a medial or skeletal linking structure $\{(M_i, U_i, \ell_i)\}$ for the configuration $\Omega = \{\Omega_i\}$ in \mathbb{R}^2 or \mathbb{R}^3 . We again let $M = \coprod_{i>0} M_i$ denote the disjoint union of the M_i for each region Ω_i for $i > 0$. Each M_i has its double \tilde{M}_i , so we introduce the double \tilde{M} for the configuration by $\tilde{M} = \coprod_{i>0} \tilde{M}_i$. For each $i > 0$, there is a canonical finite-to-one projection $\pi_i : \tilde{M}_i \rightarrow M_i$, mapping $(x, U(x)) \mapsto x$. The union of these defines a canonical projection $\pi : \tilde{M} \rightarrow M$, such that $\pi|_{\tilde{M}_i} = \pi_i$ for each $i > 0$.

We will define the skeletal integral on \tilde{M} for a multi-valued function $g : M \rightarrow \mathbb{R}$, by which we mean for any $x \in M_i$, g may have a different value for each different value of U_i at x . Such a g pulls-back via π to a well-defined map $\tilde{g} : \tilde{M} \rightarrow \mathbb{R}$ so that $g \circ \pi = \tilde{g}$.

We recall that by Proposition 3.2 of [6], for each $i > 0$, there is a positive Borel measure dM_i on \tilde{M}_i , which we call the *medial measure*. If we let $M_{i,\alpha}^{(j)}$, $j = 1, 2$, denote the inverse images of $M_{i,\alpha}$ under the canonical projection map $\pi_i : \tilde{M}_i \rightarrow M_i$, then each $M_{i,\alpha}^{(j)}$ is a copy of $M_{i,\alpha}$, representing “one side of $M_{i,\alpha}$ ” with the smoothly varying value of U_i associated to the copy. For each copy we let $dM_{ji} = \rho_{ji} dV_i$. Here dV_i denotes the Riemannian length or area on $M_{i,\alpha}$, as $n = 1$, resp. 2. Also, $\rho_{ji} = \mathbf{u}_{ji} \cdot \mathbf{n}_{ji}$ where \mathbf{u}_{ji} is a value of the unit vector field corresponding to the smooth value of U_{ji} for $M_{i,\alpha}^{(j)}$ and \mathbf{n}_{ji} is the normal unit vector pointing on the same side as U_{ji} .

Then, the integral of the multi-valued function g over $M_{i,\alpha}$ is, by definition, the sum of the integrals of the corresponding values of g over each copy $M_{i,\alpha}^{(j)}$ with respect to the medial measure dM_{ji} . It is shown in [6] that for continuous \tilde{g} , this gives a well-defined integral and this extends to integrals of “Borel measurable functions” \tilde{h} on \tilde{M}_i , which include piecewise continuous functions. Then, these distinct medial measures dM_i on \tilde{M}_i together define a *medial measure* dM on \tilde{M} ; and the integral of a Borel measurable multi-valued function g on M is defined to be

$$(4.1) \quad \int_{\tilde{M}} g dM = \sum_{i>0} \int_{\tilde{M}_i} \tilde{g} dM_i,$$

where each integral on the RHS is the integral of \tilde{g} over \tilde{M}_i with respect to the measure dM_i , and it can be viewed as an integral of g over “both sides of M_i .” If the integral is finite then we say the function is “integrable”.

We refer to the integrals in (4.1) as *medial or skeletal linking integrals*, depending on whether the linking structure is a Blum medial linking structure or a skeletal linking structure.

Computing Boundary Integrals via Medial Linking Integrals. We now show how, for a multi-object configuration with “full” Blum linking structure, we may express integrals of functions on the combined boundary \mathcal{B} as medial integrals. We emphasize that the full Blum linking structure allows the Blum medial axis to extend up to the edge-corner points of the boundaries. This does not alter the existence nor definition of the integrals, see [8, §10].

First, we consider a Borel measurable and integrable function $g : \mathcal{B} \rightarrow \mathbb{R}$ which is multi-valued in the sense that for any k -edge-corner point $x \in \mathcal{B}$, g may take distinct values for each region Ω_i , $i > 0$, containing x on its boundary. Thus, if \mathcal{B}_{ij} denotes the shared boundary region of \mathcal{B}_i and \mathcal{B}_j , g may take different values on Ω_i and Ω_j . For example, Ω_i and Ω_j may have different boundary properties such as densities measured by g .

By the integral of such a multi-valued function g over \mathcal{B} we mean

$$\int_{\mathcal{B}} g dV = \sum_{i \neq j \geq 0} \int_{\mathcal{B}_{ij}} g_{ij} dV$$

where g_{ij} denotes the values of g on \mathcal{B}_{ij} for Ω_j and dV denotes the Riemannian length (for 2D) or area (for 3D) for each \mathcal{B}_i .

Then, for the radial flow map $\psi_{i1} : \tilde{M}_i \rightarrow \mathcal{B}_i$, we define $\tilde{g} : M_i \rightarrow \mathbb{R}$ by $\tilde{g} = g \circ \psi_{i1}$, where the value on \mathcal{B}_{ij} is the value associated to Ω_i . Then, \tilde{g} is a multi-valued

Borel measurable function on M_i . We may compute the integral of g over \mathcal{B} by the following result [8, Thm 10.1].

Theorem 4.1. *Let Ω be a multi-object configuration with (full) Blum linking structure. If $g : \mathcal{B} \rightarrow \mathbb{R}$ is a multi-valued Borel measurable and integrable function, then*

$$(4.2) \quad \int_{\mathcal{B}} g dV = \int_{\tilde{M}} \tilde{g} \det(I - r_i S_{rad}) dM$$

where r_i is the radius function of each \tilde{M}_i .

In the case of a skeletal structure, there is a form of Theorem 4.1 which still applies. For each region Ω_i , with $i > 0$, let \tilde{R}_i denote a Borel measurable region of \tilde{M}_i which under the radial flow maps to a Borel measurable region R_i of \mathcal{B}_i . Let $R = \bigcup_i R_i$ and $\tilde{R} = \bigcup_i \tilde{R}_i$. We suppose that the skeletal structure satisfies the

“partial Blum condition” on \tilde{R} , by which we mean: for each i , the compatibility 1-form η_{U_i} vanishes on \tilde{R}_i (recall this means that the radial vector U_i at points of $x \in \tilde{R}_i$ is orthogonal to \mathcal{B}_i at the point where it meets the boundary). Note that for a skeletal structure this forces R to be contained in the complement of \mathcal{B}_{sing} .

Then, there is the following analogue of Theorem 4.1.

Corollary 4.2. *Let Ω be a multi-object configuration with skeletal linking structure which satisfies the partial Blum condition on the region $\tilde{R} \subset \tilde{M}$, with image R under ψ_1 . If $g : R \rightarrow \mathbb{R}$ is a multi-valued Borel measurable and integrable function, then*

$$(4.3) \quad \int_R g dV = \int_{\tilde{R}} \tilde{g} \det(I - r_i S_{rad}) dM.$$

Remark 4.3. One may compute the length (2D) or area (3D) of \mathcal{B} by choosing $g \equiv 1$ in Theorem 4.1. There is an analogous result for a region $R \subset \mathcal{B}$ which is the image of a region $\tilde{R} \subset \tilde{M}$ under the radial flow. If the configuration is modeled by a skeletal linking structure which satisfies the partial Blum condition on \tilde{R} , then the length, resp. area, of R is given by $\int_{\tilde{R}} \det(I - r_i S_{rad}) dM$.

Computing Integrals over Regions as Skeletal Linking Integrals. Next, we turn to the problem of computing integrals over regions which may be partially or completely in the external region of the configuration. Quite generally we consider a Borel measurable and integrable scalar-valued function g defined on \mathbb{R}^2 or \mathbb{R}^3 , but only nonzero on a compact region. We shall see that we can compute the integral of g as an integral of an appropriate related function on the internal skeletal sets.

Since we are in the unbounded case, we first modify the skeletal linking structure by defining ℓ_i on $M_{i,\infty}$ to be $\ell_i = \infty$. The linking flow on $M_{i,\infty}$ is a diffeomorphism for $0 \leq t < \infty (= \ell_i)$, see [8, Prop. 14.11].

Next, we replace the linking flow by a simpler *elementary linking flow* defined by $\lambda'_t(x) = x + t\mathbf{u}_i$, for $0 \leq t \leq \ell_i$ (or $< \infty$ if $\ell_i = \infty$). The elementary linking flow is again along the radial lines determined by L_i ; however, the rate differs from that for the usual linking flow. This means that the level surfaces will differ, although the images of strata under the elementary linking flow agree with that for the linking flow. In addition, as the linking flow is nonsingular, the linking curvature and edge conditions are satisfied. Then, viewing the linking vector field as a radial vector field, the radial curvature and edge curvature conditions are satisfied, and hence imply the nonsingularity of the elementary linking flow.

Then, using the elementary linking flow, we can compute the integral of g as a skeletal linking integral. We define a multi-valued function \tilde{g} on M as follows: for $x \in M_i$ with associated smooth value U_i and linking vector L_i in the same direction as U_i (so $(x, U_i) \in \tilde{M}_i$),

$$(4.4) \quad \tilde{g}(x) \stackrel{\text{def}}{=} \int_0^{\ell_i} g(\lambda'_t(x)) \det(I - tS_{rad}) dt$$

provided the integral is defined. Then, we have the following formula for the integral of g as a skeletal linking integral [8, Thm 10.6].

Theorem 4.4. *Let Ω be a multi-object configuration in \mathbb{R}^{n+1} ($n = 1$ or 2) with a skeletal linking structure. If $g : \mathbb{R}^{n+1} \rightarrow \mathbb{R}$ is a Borel measurable and integrable function which is zero off a compact region, then $\tilde{g}(x)$ is defined for almost all $x \in \tilde{M}$, it is integrable on \tilde{M} , and*

$$(4.5) \quad \int_{\mathbb{R}^{n+1}} g dV = \int_{\tilde{M}} \tilde{g} dM.$$

Remark 4.5. If we compare this formula with that given for a single region in Theorem 6.1 of [6], we notice they have a slightly different form in that a factor of ℓ_i appears to be missing. However, as noted in Remark 6.2 of that paper, it is possible to use a change of coordinates $t = \ell_i t'$ to rewrite

$$(4.6) \quad \tilde{g}(x) = \ell_i \int_0^1 g(x + t' L_i) \det(I - t' \ell_i S_{rad}) dt',$$

so that the form of (4.6) agrees with the form given in [6]. The apparent difference in form will also appear in all of the following formulas compared with the corresponding ones in [6].

Reducing to Integrals for Bounded Skeletal Linking Structures. We may replace the unbounded skeletal structure by a bounded one and replace the integrals by integrals over bounded regions. If g is zero off the compact region Q , then we may find a compact convex region $\tilde{\Omega}$ with smooth boundary containing both the configuration Ω and Q . Then, we can modify the linking structure by reducing the L_i so it is truncated where it meets $\partial\tilde{\Omega}$, the boundary of $\tilde{\Omega}$, and defining L_i on $M_{i,\infty}$ as the extensions of the radial vectors to where they meet $\partial\tilde{\Omega}$. Because the extended radial lines are transverse to $\partial\tilde{\Omega}$, the new smaller values of ℓ_i remain differentiable on the strata of each M_i . Still letting the ℓ_i denote the new smaller values, the corresponding truncated vector fields will still be denoted by L_i . Then the formula for the integral of g is still given by (4.5). We shall assume we have chosen a bounded linking structure for the remainder of this section.

To simplify the statements for the remainder of this section, we shall use the notation for a region $Q \subset \mathbb{R}^2$ or \mathbb{R}^3 : $\text{vol}_2(Q) = \text{area}(Q)$ for $Q \subset \mathbb{R}^2$ or $\text{vol}_3(Q) = \text{vol}(Q)$ for $Q \subset \mathbb{R}^3$.

For each $x \in \tilde{M}_i$, we let

$$(4.7) \quad m_Q(x) = \int_0^{\ell_i} \chi_Q(x + tL_i(x)) \det(I - tS_{rad}) dt.$$

We can view $m_Q(x)$ as a weighted 1-dimensional measure of the length of the intersection of Q with the linking line from x determined by $L_i(x)$. Then, applying Theorem 4.4 in the special case where $g \equiv 1$, we obtain an analogue of Crofton's

formula giving the area, resp. volume, of Q as a skeletal integral of m_Q using [8, Cor. 10.9].

Corollary 4.6 (Crofton Type Formula). *Let Ω be a multi-object configuration with skeletal linking structure in \mathbb{R}^{n+1} for $n = 1$, or 2. Suppose $Q \subset \mathbb{R}^{n+1}$ is a compact subset. Then*

$$(4.8) \quad \text{vol}_{n+1}(Q) = \int_{\tilde{M}} m_Q(x) dM.$$

Decomposition of a Global Integral using the Linking Flow. We next decompose the integral on the RHS of (4.5) into internal and external parts using the alternative integral representation of \tilde{g} using the linking flow. We do so by applying the change of variables formula to relate the elementary linking flow λ' with the linking flow λ , both of which flow along the linking lines but at different linear rates.

We define

$$(4.9) \quad \begin{aligned} \tilde{g}_{int}(x) &= \int_0^{r_i} g(x + t\mathbf{u}_i) \det(I - tS_{rad}) dt \quad \text{and} \\ \tilde{g}_{ext}(x) &= \int_{r_i}^{\ell_i} g(x + t\mathbf{u}_i) \det(I - tS_{rad}) dt. \end{aligned}$$

Then, we may decompose $\int g$ as follows, [8, Cor. 10.10].

Corollary 4.7. *Let Ω be a multi-object configuration in \mathbb{R}^2 or \mathbb{R}^3 with a skeletal linking structure. If $g : \mathbb{R}^{n+1} \rightarrow \mathbb{R}$ is a Borel measurable and integrable function for $n = 1$, resp. 2, which equals 0 off a compact set, then $\tilde{g}_{int}(x)$ and $\tilde{g}_{ext}(x)$ are defined for almost all $x \in \tilde{M}$, they are integrable on \tilde{M} , and*

$$(4.10) \quad \int_{\mathbb{R}^{n+1}} g dV = \int_{\tilde{M}} \tilde{g}_{int} dM + \int_{\tilde{M}} \tilde{g}_{ext} dM,$$

where

$$(4.11) \quad \int_{\tilde{M}} \tilde{g}_{int} dM = \sum_{i,j>0} \int_{M_{i \rightarrow j}} \tilde{g}_{int} dM + \sum_{i>0} \int_{M_{i,\infty}} \tilde{g}_{int} dM,$$

with an analogous formula with \tilde{g}_{int} replaced by \tilde{g}_{ext} everywhere in (4.11).

The first integral on the RHS of (4.10) is the “interior integral” of g within the configuration using the radial flow, and the second integral is the “external integral” computed using the linking flow outside of the configuration. Then we may further decompose each of these integrals using (4.11) into integrals over the distinct linking regions as illustrated in Figure 7.

Skeletal Linking Integral Formulas for Global Invariants. We now express the areas (2D) or volumes (3D) of regions associated to the linking structure, which we introduced in §3, as skeletal linking integrals. We may apply the same reasoning as in Corollary 4.6, using Corollary 4.7 to compute the volume of a compact 2D or 3D region Q as a sum of internal and external integrals.

For these calculations we will use the polynomial expression in s

$$(4.12) \quad \mathcal{I}(s) \stackrel{def}{=} \int_0^s \det(I - tS_{rad}) dt.$$

In the 2D case, $\mathcal{I}(s) = s - \frac{\kappa_r}{2}s^2$; and in the 3D case, $\mathcal{I}(s) = s - H_{rad}s^2 + \frac{1}{3}K_{rad}s^3$, where $H_{rad} = \frac{1}{2}(\kappa_{r1} + \kappa_{r2})$ and $K_{rad} = \kappa_{r1} \cdot \kappa_{r2}$, for κ_{ri} the principal radial curvatures.

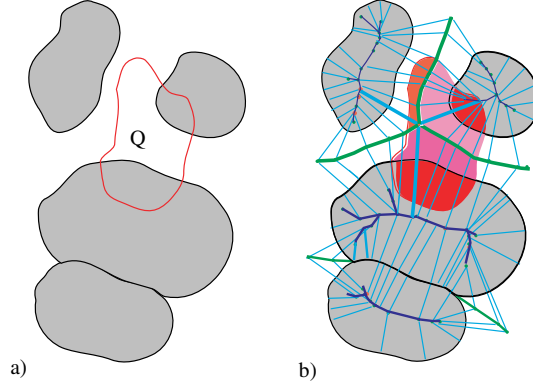


FIGURE 7. The decomposition of the integral over a region Q outlined in a) is given as the sum of integrals over regions in b) obtained by the subdivision of Q by the linking axis and the three linking lines to the branch point of the linking axis. Each $Q_{ij} \subset \mathcal{R}_{i \rightarrow j}$ (or in general including $Q_{i\infty} \subset \mathcal{R}_{i\infty}$) in the figure consists of the darker region inside the subregion $\Omega_{i \rightarrow j}$ together with the portion of Q in the linking neighborhood $\mathcal{N}_{i \rightarrow j}$. The integral can then be expressed by Corollary 4.7 as sums of internal and external integrals over the $M_{i \rightarrow j}$ and $M_{i\infty}$.

Areas and Volumes of Linking Regions as Skeletal Integrals. Then, we can express the areas or volumes of various linking regions as integrals of $\mathcal{I}(s)$ for various choices of s .

Corollary 4.8. *Let $\Omega \subset \tilde{\Omega}$ be a multi-object configuration with a bounded skeletal linking structure in R^{n+1} for $n = 1$, resp. 2. Then, the areas, resp. volumes, of linking regions in R^{n+1} are given by the following:*

$$\begin{aligned}
 \text{vol}_{n+1}(\mathcal{N}_{i \rightarrow j}) &= \int_{\tilde{M}_{i \rightarrow j}} \mathcal{I}(\ell_i) - \mathcal{I}(r_i) dM ; \\
 \text{vol}_{n+1}(\Omega_{i \rightarrow j}) &= \int_{M_{i \rightarrow j}} \mathcal{I}(r_i) dM ; \\
 \text{vol}_{n+1}(\mathcal{N}_{i, \infty}) &= \int_{M_{i, \infty}} \mathcal{I}(\ell_i) - \mathcal{I}(r_i) dM ; \\
 \text{vol}_{n+1}(\Omega_{i, \infty}) &= \int_{M_{i, \infty}} \mathcal{I}(r_i) dM .
 \end{aligned}
 \tag{4.13}$$

As well as these formulas, we can compute the volumetric invariants of other linking regions such as $\mathcal{R}_{i \rightarrow j}$, \mathcal{N}_i , etc. using skeletal linking integrals of the polynomials $\mathcal{I}(\ell_i)$ or $\mathcal{I}(r_i)$. For example,

$$\text{vol}_{n+1}(\mathcal{R}_{i \rightarrow j}) = \int_{M_{i \rightarrow j}} \mathcal{I}(\ell_i) dM ,
 \tag{4.14}$$

with an analogous formula for $\text{vol}_{n+1}(\mathcal{R}_{i, \infty})$.

As a consequence, we obtain generalizations of the classical formula of Weyl for “volumes of tubes” and Steiner’s formula for volumes of “annular regions”.

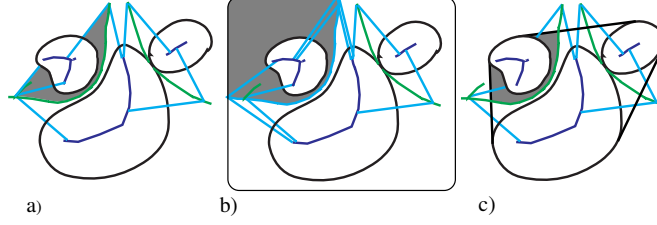


FIGURE 8. Examples of a total neighborhood $\mathcal{N}_i \cup \mathcal{N}_{i \rightarrow i} \cup \mathcal{N}_{i, \infty}$ for an object Ω_i , to which the generalized Steiner's formula applies: a) absolute threshold; b) bounding box; and c) convex hull.

Corollary 4.9 (Generalized Weyl's Formula). *Let $\Omega \subset \tilde{\Omega} \subset \mathbb{R}^{n+1}$, for $n = 1$ or 2 , be a multi-object configuration with a bounded skeletal linking structure. Then,*

$$(4.15) \quad \text{vol}_{n+1}(\Omega_i) = \int_{\tilde{M}_i} \mathcal{I}(r_i) dM.$$

The sense in which this generalizes Weyl's formula is explained for the case of a single region with smooth boundary in [6, §6, 7]. For Steiner's formula, we note that as explained in §3, $\mathcal{N}_i \cup \mathcal{N}_{i \rightarrow i} \cup \mathcal{N}_{i, \infty}$ represents the total neighborhood of Ω_i , which is the region about Ω_i extending along the linking lines. This is a generalization of an “annular neighborhood” about a region which depends on the specific type of bounding region (see Figure 8).

Corollary 4.10 (Generalized Steiner's Formula). *Let $\Omega \subset \tilde{\Omega} \subset \mathbb{R}^{n+1}$, for $n = 1$ or 2 be a multi-object configuration with a bounded skeletal linking structure. Then,*

$$(4.16) \quad \text{vol}_{n+1}(\mathcal{N}_i \cup \mathcal{N}_{i \rightarrow i} \cup \mathcal{N}_{i, \infty}) = \int_{\tilde{M}} \mathcal{I}(\ell_i) - \mathcal{I}(r_i) dM.$$

Remark 4.11. The regions in both generalizations of Weyl's formula and Steiner's formula for different i and j will only intersect in lower dimensional regions. Thus, in both cases we can sum the integrals on the RHS for multiple i to obtain formulas for a union of Ω_i .

5. POSITIONAL PROPERTIES OF MULTI-OBJECT CONFIGURATIONS

In this section we define positional geometric invariants of configurations in terms of volumetric measures of associated regions defined by the linking structure. We emphasize that the volumetric measures versus boundary measures of positional geometry have two advantages: 1) they are computable from the skeletal linking structure, and unlike surface measures, they do not require the partial Blum condition to compute the invariants; and 2) as in Figure 5, the volumetric invariants capture the total geometric structure of regions better than boundary measures.

We proceed as follows. We first use the linking structure to determine which of the objects should be regarded as neighboring objects. Then, we use the regions associated to the linking structure to define invariants which measure the closeness of such neighboring objects. Second, we further introduce numerical invariants measuring the positional significance of objects for the configuration. These allow us to identify which objects are central to the configuration and which ones are peripheral.

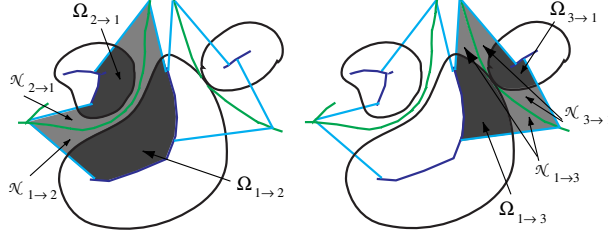


FIGURE 9. Measure of closeness for regions in the configuration in b) of Figure 6 bounded via a threshold with the bounded skeletal linking structure. For a pair of neighboring regions Ω_i and Ω_j , $c_{i \rightarrow j}$ denotes the ratio of the volume of the darker region $\text{vol}(\Omega_{i \rightarrow j})$ and the volume of the total shaded region $\text{vol}(\mathcal{R}_{i \rightarrow j}) = \text{vol}(\Omega_{i \rightarrow j}) + \text{vol}(\mathcal{N}_{i \rightarrow j})$.

In §6 we will use the closeness measures to construct a “proximity matrix” which yields proximity weights for the objects based on their closeness to other objects. We also will use both types of invariants to construct a *tiered linking graph*, with vertices representing the objects, and edges between vertices representing neighboring objects, with the closeness and significance values assigned to the edges, resp. vertices. By applying threshold values to this structure we can exhibit the subconfigurations within the given thresholds.

Neighboring Objects and Measures of Closeness. We consider a configuration $\Omega = \{\Omega_i\} \subset \tilde{\Omega}$, with a bounded skeletal linking structure. We use linking between objects Ω_j and Ω_i as a criterion for their being neighbors, so that objects which are not linked are not considered neighbors. The simplest measure of closeness between neighboring objects is the minimum distance between the objects. However, this ignores the size of the objects and how big a portion of each object is close to the other object, as illustrated in Figure 2 where Ω_3 is close to Ω_1 for a small region but Ω_2 is close to Ω_1 over a larger region. Moreover, if we choose a more global definition of closeness involving all neighboring boundary points, then as in Figure 5, this will not measure the portions of the objects which are close. We do overcome both of these issues by using volumetric measures of appropriate regions defined using the linking structures.

For a configuration Ω with a skeletal linking structure, we introduced in §3 regions $\Omega_{i \rightarrow j}$ and $\Omega_{j \rightarrow i}$ which capture the neighbor relations between Ω_i and Ω_j . Since $\mathcal{N}_{i \rightarrow j}$ and $\mathcal{N}_{j \rightarrow i}$ share a common boundary region in M_0 , they are both empty if one is, and then both $\Omega_{i \rightarrow j}$ and $\Omega_{j \rightarrow i}$ are empty. In that case Ω_i and Ω_j are not linked. Otherwise, we may introduce a measure of closeness.

There are two different ways to do this, each having a probabilistic interpretation. First, we let

$$c_{i \rightarrow j} = \frac{\text{vol}(\Omega_{i \rightarrow j})}{\text{vol}(\mathcal{R}_{i \rightarrow j})} \quad \text{and} \quad c_{i j} = c_{i \rightarrow j} \cdot c_{j \rightarrow i}.$$

Then, $c_{i \rightarrow j}$ is the probability that a point chosen at random in $\mathcal{R}_{i \rightarrow j}$ will lie in Ω_i (see Figure 9); so $c_{i j}$ is the probability that a pair of points, one each in $\mathcal{R}_{i \rightarrow j}$ and $\mathcal{R}_{j \rightarrow i}$ both lie in the corresponding regions Ω_i and Ω_j .

Note that c_{ij} contains much more information than the closest distance between Ω_i and Ω_j , and even the “ L^1 -measure” of the region between Ω_i and Ω_j . It compares this measure with how much of the regions Ω_i and Ω_j are closest as neighbors. If both $\Omega_{i \rightarrow j}$ and $\Omega_{j \rightarrow i}$ are empty, we let $c_{i \rightarrow j}$, $c_{j \rightarrow i}$, and $c_{ij} = 0$. Also, we let $c_{ii} = 1$. Thus, from the collection of values $\{c_{ij}\}$ we can compare the closeness of any pair of regions.

Since these invariants depend on a bounded skeletal linking structure, one way to introduce a parametrized family $c_{ij}(\tau)$ is by considering the varying threshold values τ . For example, τ may represent the maximum allowable values for ℓ_i or the maximum value of ℓ_i relative to some intrinsic geometric linear invariant of Ω_i . As τ increases, the bounded region increases and how $c_{ij}(\tau)$ varies indicates how the closeness of the regions varies when larger linking values are taken into account. Thus, this provides a method to use the local properties of the skeletal linking structure to introduce a scale of local closeness.

A second way to introduce a measure of closeness is to use an “additive contribution” from each region and define

$$c_{ij}^a = \frac{\text{vol}(\Omega_{i \rightarrow j}) + \text{vol}(\Omega_{j \rightarrow i})}{\text{vol}(\mathcal{R}_{i \rightarrow j}) + \text{vol}(\mathcal{R}_{j \rightarrow i})}.$$

Here c_{ij}^a is the probability that a point chosen in the region $\mathcal{R}_{i \rightarrow j} \cup \mathcal{R}_{j \rightarrow i}$ lies in the configuration, i.e. in $\Omega_i \cup \Omega_j$. We also let $c_{ij}^a = 0$ if Ω_i and Ω_j are not linked; and we let $c_{ii}^a = 1$. Again, to obtain a more precise measure of closeness, we can vary a measure of threshold τ and obtain a varying family $c_{ij}^a(\tau)$. The invariants satisfy $0 \leq c_{ij}, c_{ij}^a \leq 1$. The value 0 indicates no linking, for values near 0, the regions are neighbors but distant so they are “weakly linked,” and for values close to 1, the regions are close over a large boundary region and are “strongly linked.”

There is a simple but crude relation between c_{ij}^a and the pair $c_{i \rightarrow j}$ and $c_{j \rightarrow i}$:

$$c_{ij}^a \leq c_{i \rightarrow j} + c_{j \rightarrow i}.$$

As $c_{ij}^a \leq 1$, this is only useful when the two regions are weakly linked.

Measuring Positional Significance of Objects Via Linking Structures. In order to measure *positional significance* of an object among a collection of objects, we can think in both absolute and relative terms. In each case, we emphasize that we are considering a form of geometric significance of objects relative to the configuration, rather than some other notion such as significance in the sense of statistics. We begin with the relative version. Given Ω_i , we define the *positional significance measure*

$$s_i = \frac{\sum_{j \neq i} \text{vol}(\Omega_{i \rightarrow j})}{\sum_{j \neq i} \text{vol}(\mathcal{R}_{i \rightarrow j})}.$$

It takes values $0 \leq s_i \leq 1$. For values near 0, the portion of the region of Ω_i linked to other regions is a small fraction of the external region between Ω_i and the other regions. Thus, compared to its size it is distant from other neighboring objects, so it is a peripheral region of the configuration. We would have the value $s = 0$ if Ω_i is not linked to any other region in Ω , which may occur if there is a threshold for which the region is not linked to another region with a linking vector of length less than the threshold. By contrast, if s_i is close to 1, then there is very little external region between Ω_i and the other regions. Thus, Ω_i is central for the configuration,

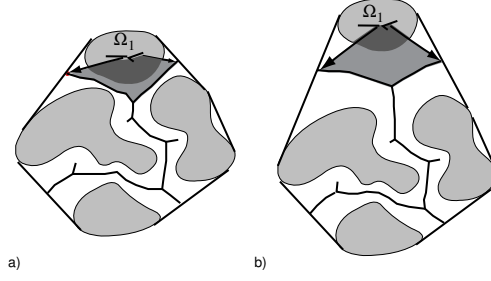


FIGURE 10. For Ω_1 in configurations using convex hull bounding regions, a measure of positional significance is the ratio of the darkest region to the union of the two more darkly shaded regions. In a) Ω_1 is central, while in b) when Ω_1 is moved away from the remaining regions, the ratio decreases indicating it is becoming more peripheral to the configuration.

see Figure 10. Note that

$$s_i \leq \sum_{j \neq i} c_{i \rightarrow j},$$

so that Ω_i being weakly linked to the other regions implies it has small significance for the configuration. If we would like to further base the positional significance of the region Ω_i on its absolute size, we can alternatively use an absolute measure of positional significance defined by $\tilde{s}_i = s_i \text{vol}(\Omega_i)$. Then, the effect of the smallness of s_i will be partially counterbalanced by the size of Ω_i .

Properties of Invariants for Closeness and Positional Significance. We consider three properties of these invariants:

- 1) computation of all of the invariants as skeletal linking integrals;
- 2) invariance under the action of the Euclidean group and scaling; and
- 3) continuity of the invariants under small perturbations of generic configurations.

Computation of the Invariants as Skeletal Linking Integrals. We can use the results from the previous section to compute as skeletal linking integrals the above volumes of regions associated to Ω . This is summarized by the following, see [8, Thm. 11.3].

Theorem 5.1. *If $\Omega = \{\Omega_i\} \subset \tilde{\Omega} \subset \mathbb{R}^{n+1}$, for $n = 1$ or 2 is a multi-object configuration, with a bounded skeletal linking structure, then all global invariants of the configuration which can be expressed as integrals over regions in \mathbb{R}^2 , resp. \mathbb{R}^3 , can be computed as skeletal linking integrals using Theorem 4.4. In particular, the invariants $c_{i \rightarrow j}$, c_{ij} , c_{ij}^a , and s_i are given as the quotients of two skeletal linking integrals using (4.13) and (4.14).*

Remark 5.2. We emphasize that we could try to alternatively use boundary measures for the regions to define closeness and significance. There are two problems with this approach. From a computational point of view, the skeletal structures could only be used where the partial Blum condition is satisfied. Moreover, boundary measures do not capture how much of the regions are close to each other (only where their boundaries are close). For these reasons we have concentrated on (ratios of) volumetric measures to capture positional geometry of the configuration.

Invariance Under the Action of the Euclidean Group and Scaling. Second, we establish the invariance of the invariants defining closeness and significance under Euclidean motions and scaling. Let $\Omega = \{\Omega_i\} \subset \tilde{\Omega} \subset \mathbb{R}^{n+1}$, for $n = 1$ or 2 be a multi-object configuration, with a bounded skeletal linking structure $\{(M_i, U_i, \ell_i)\}$. If f is a Euclidean motion and $a > 0$ is a scaling factor, then we may let $\Omega' = \{\Omega'_i\} \subset \tilde{\Omega}'$, where $\Omega'_i = f(\Omega_i)$ and $\tilde{\Omega}' = f(\tilde{\Omega})$. We also let $\{(M'_i, U'_i, \ell'_i)\}$ be a skeletal linking structure for Ω' defined by $M'_i = f(M_i)$, $U'_i = f(U_i)$, and $\ell'_i = \ell_i$. As f preserves distance and angles, we have $r'_i = r_i$, and the image of the linking flow for Ω is the linking flow for Ω' . Then, $\{(M'_i, U'_i, \ell'_i)\}$ satisfies the conditions for being a skeletal linking structure for Ω' . As $\tilde{\Omega}' = f(\tilde{\Omega})$, the corresponding bounded linking structure for Ω' using $\tilde{\Omega}'$ is the image of that for Ω for $\tilde{\Omega}$. Then, the associated linking regions for Ω' are the images of the corresponding associated linking regions for Ω . Since f preserves volumes, the invariants for closeness and significance are preserved by f .

If instead we consider a scaling by the factor $a > 0$, then we let $g_a(x) = a \cdot x$. Now the images of Ω and $\tilde{\Omega}$ under g_a define a configuration Ω' in $\tilde{\Omega}'$. We likewise let $\{(M'_i, U'_i, \ell'_i)\}$ be defined by $M'_i = g_a(M_i)$, $U'_i = aU_i$, and $\ell'_i = a\ell_i$ (and $r'_i = ar_i$). As before this is a skeletal structure for Ω' . Everything goes through except that g_a multiplies volume by a^{n+1} , $n = 1, 2$. However, as the invariants are ratios of volumes, they again do not change. We summarize this with the following.

Proposition 5.3. *If $\Omega = \{\Omega_i\} \subset \tilde{\Omega} \subset \mathbb{R}^{n+1}$, for $n = 1$ or 2 is a multi-object configuration, with a skeletal linking structure, then the invariants $c_{i \rightarrow j}$, c_{ij} , c_{ij}^a , and s_i are invariant under the action of Euclidean motion and scaling applied to both Ω and $\tilde{\Omega}$ for the image of the skeletal linking structure for the image configuration and bounding region.*

We note that if we consider the absolute significance \tilde{s}_i , then it is still invariant under Euclidean motions. However, under scaling by $a > 0$, it changes by the factor a^{n+1} for $n = 1, 2$; but this would not alter the hierarchy based on absolute significance, as all \tilde{s}_i would be multiplied by the same factor.

Remark 5.4. Importantly, the invariance in Proposition 5.3 crucially depends on also applying the Euclidean motion and/or scaling to the bounding region $\tilde{\Omega}$. For either thresholds or convex hulls, there is no problem. If instead the bounding region is either fixed, or depends upon an external condition which prevents it from transforming along with the configuration, then the invariance does not hold. The change under Euclidean motion f or scaling by a could be measured in terms of the changes in the portions of the linking regions that lie in the difference region between $\tilde{\Omega}$ and its image under f or scaling.

Continuity and Changes Under Small Perturbations. Lastly, suppose that the configuration $\Omega = \{\Omega_i\} \subset \tilde{\Omega}$ has a skeletal linking structure. We ask how will the invariants change under small perturbations?

First, if objects undergo a sufficiently small deformation, then we may deform the skeletal linking structure to be the skeletal linking structure for the deformed configuration, in such a way that the skeletal structures and linking vector fields will deform in a strata-wise differentiable fashion. Then, the associated regions will also deform in a piecewise differentiable fashion. Hence, the volumes of these regions will vary continuously. Thus, the quotients of the volumes will also vary continuously.

It then follows that the invariants, which are quotients of such volumes will also vary continuously.

How exactly they will vary will depend on the particular deformation. For example, suppose we enlarge one of the regions Ω_i by increasing the radial vectors by a factor $a > 1$, so that $ar_i < \ell_i$, and without altering the remainder of the skeletal structure. If the region remains in the bounding region and doesn't intersect itself or other regions, then the ratio $\text{vol}(\Omega_{i \rightarrow j})$ to $\text{vol}(\mathcal{R}_{i \rightarrow j})$ will increase for each j so the s_i will increase, as will the $c_{i \rightarrow j}$. If instead $0 < a < 1$, then s_i and $c_{i \rightarrow j}$ will decrease. If we move the region Ω_i in a direction away from all of the other regions without altering its size, then in general s_i will decrease, and conversely if we move it toward the other regions, generally s_i will increase. Thus, the changes in the invariants capture the changes in the configuration resulting from the deformation.

6. PROXIMITY MATRIX AND TIERED LINKING GRAPH FOR MULTI-OBJECT CONFIGURATIONS

The invariants we introduced in the previous section individually capture positional properties of objects in a configuration. We show how they taken together provide numerical structures which summarize the relations in the configuration. These take two forms: a *proximity matrix* that has a unique positive eigenvalue with eigenvector with positive entries assigning unique *proximity weights* to the objects based on their relative closeness; and a *tiered linking graph* structure, which identifies substructures satisfying threshold conditions.

Proximity Matrix and Proximity Weights. We consider a configuration $\Omega = \{\Omega_i\}$ with a bounded skeletal linking structure. If there are n objects, we let P be the $n \times n$ matrix with entries c_{ij} given in the previous section (or instead with c_{ij}^a). We refer to P as the *proximity matrix*. The proximity matrix purely measures the relative amounts of two objects which are neighbors compared with their adjacent regions. We can further weight the proximity matrix to take into account the size of the objects. If for each i , $V_i > 0$ is a measure of the object Ω_i , and we let $V_{tot} = \sum_{i=1}^n V_i$, then for $v_i = \frac{V_i}{V_{tot}}$, the vector $\mathbf{v} = (v_1, v_2, \dots, v_n)$ is a positive weight vector for the relative portion each Ω_i contributes to the total measure V_{tot} . Two possibilities for V_i are either the total volume/area $\text{vol}(\Omega_i)$, yielding the vector \mathbf{v}_{vol} or instead $V_i = \sum_{j \neq i} \text{vol}(\Omega_{i \rightarrow j})$, the portion of Ω_i which is linked to some other object in the configuration, yielding \mathbf{v}_{lk} . Then, we can form the *renormalized proximity matrix* $\tilde{P} = (c_{ij} \frac{v_i}{v_j})$. The proximity and renormalized proximity matrices yield *proximity weights* and *renormalized proximity weights* for the objects in the configuration as follows.

Proposition 6.1. *Consider a configuration of objects $\Omega = \{\Omega_i\}$ with a bounded skeletal linking structure, such that within a bounding region there is no subset of objects all of which are unlinked to the complementary set of objects in the configuration. Then,*

- i) *both the proximity matrix and renormalized matrix have the same unique maximal positive eigenvalue λ_P with an eigenvector \mathbf{w} for P and $\tilde{\mathbf{w}}$ for \tilde{P} both having all positive entries;*
- ii) *this is the only eigenvalue for either matrix with an eigenvector with these properties; and*

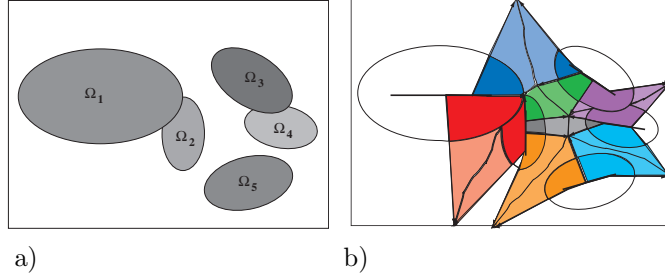


FIGURE 11. In a) is a synthetic configuration of 5 objects in a bounding window. In b) is the decomposition of the neighboring regions based on a Blum linking structure which is deformed at the singular points of the boundaries. The subregions $\Omega_{i \rightarrow j}$ and $\Omega_{j \rightarrow i}$ of different objects Ω_i and Ω_j which are linked have the same color, and the external linking regions $\mathcal{N}_{i \rightarrow j}$ and $\mathcal{N}_{j \rightarrow i}$ have the same lighter color. The white regions of objects are unlinked in the bounding window. The values for closeness, significance, the proximity matrix, the proximity weights and the renormalized proximity weights in Example 6.2 are computed from this figure.

- iii) if $\mathbf{w} = (w_1, \dots, w_n)$ is such an eigenvector for P , then $\tilde{\mathbf{w}} = (w_1 V_1, \dots, w_n V_n)$ is such an eigenvector for \tilde{P} .

Since \mathbf{w} and $\tilde{\mathbf{w}}$ are only well-defined up to positive scalar multiples, we may normalize each to vectors $\mathbf{w}_P = (w_1, \dots, w_n)$, resp. $\tilde{\mathbf{w}}_P = (\tilde{w}_1, \dots, \tilde{w}_n)$ with $\sum_{i=1}^n w_i = 1$, resp. $\sum_{i=1}^n \tilde{w}_i = 1$. Thus, each vector uniquely assigns a weight w_i , resp. \tilde{w}_i , to the object Ω_i depending on the proximity of the other regions to it. We refer to these weights as the *proximity weights*, resp. *renormalized proximity weights* for the objects in the configuration. The proximity weights uniquely provide an ordering on the objects based on their proximity to other objects, with the renormalized weights modifying this weighting to include a measure of the size of the objects.

Proof. By the properties of the closeness measures c_{ij} , the matrix P has the properties that it is a symmetric nonnegative matrix. Moreover, because of the properties of the configuration in the bounding region, the matrix P is “irreducible”, which for nonnegative symmetric matrices reduces to the condition that for any i there is a $j \neq i$, such that $c_{ij} \neq 0$. Then we may apply a version of the Perron-Frobenius theorem for irreducible nonnegative matrices, see e.g. [13] or [20, Chap. 8], to conclude there is a unique largest positive eigenvalue λ_P for P with eigenvector \mathbf{w} with all positive entries. Moreover, this is the only eigenvalue with an eigenvector with these properties.

As P is irreducible, so is \tilde{P} , which is conjugate to P by a diagonal matrix with values $\frac{1}{v_i}$ on the diagonal. Furthermore it follows that the eigenvalues of \tilde{P} are the same as those of P , and for a common eigenvalue λ , with the eigenvector $\mathbf{w} = (w_1, \dots, w_n)$ for P , there is a corresponding eigenvector $\tilde{\mathbf{w}} = (w_1 V_1, \dots, w_n V_n)$ for \tilde{P} . Thus, the results also follow for \tilde{P} . \square

Example 6.2. In a) of Figure 11 is a synthetic configuration of 5 objects in a bounding window in \mathbb{R}^2 . In this case “vol” refers to the area of the various regions. The positional invariants are computed using the linking regions and neighborhoods indicated in b) of Figure 11. This yields: the proximity matrix P given in (6.1) and in (6.3) the normalized measures for either the areas of the individual object regions, \mathbf{v}_{vol} , or the areas of the total internal linking regions for each object, \mathbf{v}_{lk} , and the positional significance vector \mathbf{s} consisting of the positional significance value for each object.

$$(6.1) \quad P = \begin{pmatrix} 1 & .240 & .081 & 0 & 0 \\ .240 & 1 & .200 & .104 & .152 \\ .081 & .200 & 1 & .487 & 0 \\ 0 & .104 & .487 & 1 & .305 \\ 0 & .152 & 0 & .305 & 1 \end{pmatrix}$$

The proximity weight vector given by Proposition 6.1 is computed to be

$$(6.2) \quad \mathbf{w}_P = (0.10, 0.19, 0.26, 0.28, 0.17).$$

We first note that despite Ω_1 having by far the largest area, its weight when determined from pure closeness data is small compared to the other objects. This is because as we see in b) of Figure 11, most of Ω_1 is unlinked and hence effectively invisible to the other objects. By contrast, a much greater portion of Ω_3 and Ω_4 plays a central role in the configuration. We compare these weights with the renormalized weights using the weight vectors \mathbf{v}_{vol} and \mathbf{v}_{lk} given by (6.3).

$$(6.3) \quad \begin{aligned} \mathbf{v}_{vol} &= (0.49, 0.11, 0.15, 0.10, 0.15), \\ \mathbf{v}_{lk} &= (0.34, 0.21, 0.10, 0.16, 0.19), \\ \mathbf{s} &= (0.52, 0.40, 0.43, 0.46, 0.49). \end{aligned}$$

Using the weight vectors \mathbf{v}_{vol} and \mathbf{v}_{lk} given by (6.3), we obtain the renormalized weight vectors for the configuration in (6.4)

$$(6.4) \quad \begin{aligned} \tilde{\mathbf{w}}_{P, vol} &= (0.30, 0.12, 0.24, 0.19, 0.15), \\ \tilde{\mathbf{w}}_{P, lk} &= (0.18, 0.22, 0.15, 0.27, 0.18). \end{aligned}$$

We now see that using the vector \mathbf{v}_{lk} , using areas of the linked regions of the objects, the weight of Ω_1 increases and Ω_3 significantly decreases, while the others change only slightly. If instead we renormalize by the total areas of the objects given by \mathbf{v}_{vol} , then the overall importance of Ω_1 , as measured by its size becomes evident in $\tilde{\mathbf{w}}_P$. Thus, the three vectors \mathbf{w}_P , $\tilde{\mathbf{w}}_{P, vol}$, and $\tilde{\mathbf{w}}_{P, lk}$ give different measures of the weights of the objects within the configuration, successively increasing the importance attached to the size of the objects involved in the configuration. We may compare these three measures with the positional significance measure given in \mathbf{s} in (6.3), where despite the differences in size, number of neighbors, and linking structures, the calculated significance measures for all five objects are within a narrow range $0.4 \leq s_i \leq 0.52$.

Viewing b) of Figure 11, we remark that alternative methods that would reduce the effect of the triangular regions reaching out to the boundary would be either to use a threshold for the linking functions ℓ_i or use the convex hull of the configuration as the bounding region as described in [9, §3].

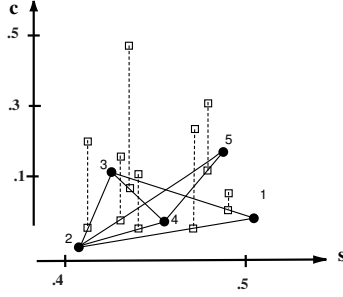


FIGURE 12. Example of the tiered graph structure for the configuration in Example 6.2 shown in Figure 11. The horizontal axis indicates positional significance s , and closeness c_{ij} is given by the values of the height function on the edges indicated by the tops of the dotted lines.

Tiered Linking Graph. We can furthermore use the invariants c_{ij} and s_i in a second way to construct a *tiered graph* which simultaneously captures both the relative positions of the objects and their significance for the configuration. For us a graph Γ is defined by a finite set of vertices $V = \{v_i : i = 1, \dots, m\}$, and a set of unordered edges $E = \{e_{ij}\}$ with at most one edge e_{ij} between any pair of distinct vertices v_i and v_j .

Definition 6.3. A *tiered graph* consists of a graph Γ together with a discrete nonnegative function $f : V \cup E \rightarrow \mathbb{R}_+$ which we shall more simply denote by $f : \Gamma \rightarrow \mathbb{R}_+$. The discrete function f has values $f(v_i) = a_i \geq 0$ for each vertex v_i , and $f(e_{ij}) = b_{ij} \geq 0$ for each edge e_{ij} .

Given such a tiered graph, we can view its values on vertices and edges as height functions assigning weights to the vertices and edges; and then apply “thresholds” to f to identify subgraphs, distinguished vertices and edges. First, given a value $b > 0$, we can consider the subgraph Γ_b consisting of all vertices, but only those edges where $f \geq b$. Γ_b decomposes into connected subgraphs consisting of vertices which have edges of weights $> b$. As b decreases from $B = \max\{b_{ij}\}$, then we see the smaller graphs begin to merge as edges are added, until we reach Γ for $b = \min\{b_{ij}\}$.

If instead we consider the threshold a for f on vertices, then instead we define Γ^a to consist of those vertices with $f \geq a$, and only those edges joining two vertices within this set. This identifies a subgraph consisting of the most important vertices as measured by weights, along with the edges between these vertices. Again as a decreases from $A = \max\{a_i\}$, then again we see the small graphs being supplemented by additional vertices with edges being added from these vertices until we reach the full graph when $a = \min\{a_i\}$. This gives a hierarchical structure to the graph Γ . Along with the subgraphs and the hierarchical structure, we can also identify vertices which are joined by strongly weighted edges, and important vertices with large weights a_i , and less significant ones with small weights a_i .

This approach, using the tiered graph structure, applies to a configuration of multiple objects with a skeletal linking structure. We define the associated *tiered linking graph* Λ as follows. For each object Ω_i , we assign a vertex v_i in Λ , and to each pair of neighboring objects Ω_i and Ω_j , we assign an edge e_{ij} joining the

corresponding vertices. If the objects are not neighbors, there is no edge. We define the height function f by: $f(v_i) = s_i$ and $f(e_{ij}) = c_{ij}$ (or c_{ij}^a).

An example is shown in Figure 12 for the configuration in Example 6.2 using the closeness and positional significance measures computed in the proximity matrix P and positional significance vector \mathbf{s} . When we apply the thresholds, we remove vertices to the left of some vertical line or edges whose heights are below some height. We see how subconfigurations associated to the subgraphs merge into larger configurations as the vertical line indicating s moves to the right adding objects, or the height moves downwards, adding edges, with the resulting graphs being based on closeness or significance of the subconfigurations of objects. Position along the s -axis identifies the hierarchy of objects in the configuration.

For Example 6.2, in Figure 12 we see that while Ω_1 has the greatest positional significance measure, the combined position and size of Ω_5 places it second. Also, as we move upward along the closeness scale we remove edges; so for example, as we move above the closeness threshold of 0.2, we see the subconfigurations of $\{\Omega_1, \Omega_2\}$ and $\{\Omega_3, \Omega_4, \Omega_5\}$ appearing.

Concluding Remarks. Presently, the investigation of configurations of objects in images typically involves many ad hoc choices. To approach such collections in a systematic way, there is needed a uniform approach based on structures whose properties allow investigators to associate numerical measures which capture geometric features of the configuration and which can then be compared for statistical purposes for various image processing goals. In this paper we have made use of a medial/skeletal linking structure to model such a configuration, as introduced in [9]. Using this structure we introduced a number of numerical invariants which capture positional geometry of the configuration, along with the geometric properties of the individual objects in the configuration. These yield a collection of mathematical tools that have already been successfully applied to single objects in medical images and now have a rigorous mathematical form for being applied to entire configurations of objects.

REFERENCES

- [1] H. Blum and R. Nagel, *Shape description using weighted symmetric axis features*, Pattern Recognition **10** (1978), 167–180.
- [2] E. Chaney, S. Pizer, et al., *Automatic Male Pelvis Segmentation from CT Images via Statistically Trained Multi-Object Deformable M-rep Models*, Amer. Soc. Therapeutic Radiology and Oncology (ASTRO) (2004).
- [3] J. Damon, *Smoothness and Geometry of Boundaries Associated to Skeletal Structures I: Sufficient Conditions for Smoothness*, Annales Inst. Fourier **53** (2003), 1001–1045.
- [4] ———, *Smoothness and Geometry of Boundaries Associated to Skeletal Structures II: Geometry in the Blum Case*, Compositio Mathematica **140** (6) (2004), 1657–1674.
- [5] ———, *Determining the Geometry of Boundaries of Objects from Medial Data*, Int. Jour. Comp. Vision **63** (1) (2005), 45–64.
- [6] ———, *Global Geometry of Regions and Boundaries via Skeletal and Medial Integrals*, Comm. Anal. and Geom. **15** (2) (2007), 307–358.
- [7] ———, *Geometry and Medial Structure*, chapter in *Medial Representations: Mathematics, Algorithms, and Applications*, S. Pizer and K. Siddiqi, Editors, **37** Comp. Imaging and Vision, Springer-Verlag (2008) 69–123
- [8] J. Damon and E. Gasparovic, *Medial/Skeletal Linking Structures for Multi-Region Configurations*, 135 pages, to appear Memoirs Amer. Math. Soc. (available <http://arxiv.org/abs/1402.5517v2>)

- [9] ———, *Modeling Multi-Object Configurations via Medial/Skeletal Linking Structures*, submitted for publication.
- [10] E. Gasparovic, *The Blum Medial Linking Structure for Multi-Region Analysis*, Ph.D. Thesis, Dept. of Mathematics, Univ. of North Carolina at Chapel Hill, 2012.
- [11] P.J. Giblin, *Symmetry Sets and Medial Axes in Two and Three Dimensions*, The Mathematics of Surfaces, Roberto Cipolla and Ralph Martin (eds.), Springer-Verlag (2000), 306–321.
- [12] P.J. Giblin, B.B. Kimia, *A formal classification of 3D medial axis points and their local geometry*, IEEE Trans. Pattern Anal. Mach. Intell. **26** (2) (2004), 238–251.
- [13] Gantmacher, F. *Theory of Matrices*, **2**, AMS Chelsea publ. 2000
- [14] K. Gorczowski, M. Styner, J-Y. Jeong, J.S. Marron, J. Piven, H.C. Hazlett, S.M. Pizer, G. Gerig, *Multi-Object Analysis of Volume, Pose, and Shape Using Statistical Discrimination*, IEEE TPAMI **32** (4) (2010), 652–661.
- [15] J. Jeong, S. Pizer, and S. Ray, *Statistics on Anatomic Objects Reflecting Inter-Object Relations*, MICCAI (2006).
- [16] J. Jeong, J. Stough, S. Marron, and S. Pizer, *Conditional-Mean Initialization Using Neighboring Objects in Deformable Model Segmentation*, SPIE (2008).
- [17] B. B. Kimia, A. Tannenbaum, and S. Zucker, *Toward a computational theory of shape: An overview*, O. Faugeras ed., Three Dimensional Computer Vision, MIT Press, 1990.
- [18] C. Lu, S. Pizer, S. Joshi, and J. Jeong, *Statistical Multi-Object Shape Models*, Int. Jour. Comp. Vision **75** (3) (2007), 387–404.
- [19] J. Mather, *Distance from a Submanifold in Euclidean Space*, in Proc. Symp. Pure Math. **40** Pt 2 (1983), 199–216.
- [20] C. Meyer, *Matrix Analysis and Applied Linear Algebra*, SIAM publ. 2000
- [21] S. Musuvathy, E. Cohen, and J. Damon, *Computing the Medial Axis for Generic 3D Regions Bounded by B-Spline Surfaces*, Computer Aided Design **43** (11) (2011), 1485–1495.
- [22] S. Pizer et al., *Multiscale Medial Loci and their Properties*, Int. Jour. Comp. Vision **55** no. 2-3 (2003), 155–179.
- [23] S. Pizer et al., *Deformable M-reps for 3D Medical Image Segmentation*, Int. Jour. Comp. Vision **55** (2) (3) (2003), 85–106.
- [24] S. Pizer and K. Siddiqi, Editors, *Medial Representations: Mathematics, Algorithms, and Applications*, **37** Computational Imaging and Vision, Springer-Verlag, 2008.
- [25] K. Siddiqi, S. Bouix, A. Tannenbaum and S. Zucker, *The Hamilton–Jacobi Skeleton*, Int. Jour. Comp. Vision **48** (2002), 215–231.
- [26] H. Weyl, *On the Volume of Tubes*, Amer. Jour. Math. **61** (1939), 461–472.
- [27] J. Yomdin, *On the Local Structure of the Generic Central Set*, Compositio. Math. **43** (1981), 225–238.

DEPT. OF MATHEMATICS, UNIVERSITY OF NORTH CAROLINA, CHAPEL HILL, NC 27599-3250
E-mail address: jndamon@math.unc.edu

DEPT. OF MATHEMATICS, UNION COLLEGE, SCHENECTADY, NY 12308
E-mail address: gasparoe@union.edu